Hindawi
Advances in Materials Science and Engineering
Volume 2020, Article ID 8167386, 11 pages
https://doi.org/10.1155/2020/8167386

Research Article

The Enhanced Performance of Phase-Change Materials via 3D Printing with Prickly Aluminum Honeycomb for Thermal Management of Ternary Lithium Batteries

Ming Cao, Juhua Huang, and Ziqiang Liu

School of Mechatronics Engineering, Nanchang University, Nanchang 330031, China

Correspondence should be addressed to Ziqiang Liu; 15779708915@163.com

Received 27 December 2019; Accepted 4 February 2020; Published 9 March 2020

Academic Editor: Yi Huang

This study introduces a new type of lightweight, shape-stable composite phase-change material (CPCM) to improve the thermal management of ternary lithium batteries. Paraffin wax (PW) was used as a phase-change material, expanded graphite (EG) and high-density polyethylene (HDPE) were used as support materials, carbon fiber (CF) was used as a heat-conductive additive, and a 3D printed aluminum honeycomb with a prickly structure (3D Al-Hc) was added to enhance the mechanical properties and thermal conductivity of the CPCM. The properties of the CPCM were analyzed based on its microstructure, thermal properties, and stress-strain response. The CPCM was applied to a battery cooling module to determine the temperature response of a battery. The results showed that when the CF mass fraction was 4.5 wt%, the degree of supercooling in the PW/EG/CF/HDPE was reduced by 51.5% and 43.3% compared to PW PCM and PW/EG CPCM, respectively. In addition, the thermal conductivity of the PW/EG/CF/HDPE/3D AL-Hc CPCM (5.723 W/(m·K)) was 1.9 times that of the PW/EG. Due to the presence of the 3D AL-Hc, the CPCM has a strain of 1.25 mm at a pressure of 100 KPa. In addition, the CPCM has excellent battery thermal management performance. At a 2.5°C discharge rate, the operating temperature of the battery is kept within the safe temperature range of 50°C.

1. Introduction

In order to overcome the energy crisis and environmental pollution caused by traditional cars, new energy vehicles are needed to replace traditional cars. Although the power battery is one of the three major components of electric vehicles, it is very sensitive to temperature and generates a lot of heat during operation. If the battery does not dissipate in time and is frequently operated at high temperatures, it will greatly reduce its reliability and service life [1]. Therefore, an efficient thermal management system is needed to ensure efficient battery operation.

Traditional battery thermal management (BTM) technologies include forced air cooling [2, 3], liquid cooling [4, 5], and phase-change material cooling [6, 7]. Among these, the phase-change material has been widely concerned because of its low costs, high efficiency, and simple and compact structure [8]. Phase-change materials (PCMs) mainly include organic materials [9–11] such as paraffin, fatty acids, and inorganic materials [12–14], such as crystalline hydrated salts and molten salts. In the BTMS, PW is considered to be one of the best phase-change materials due to its large latent heat capacity, small volume change, slight supercooling, and low costs. However, the low thermal conductivity of paraffin, the liquid phase leakage during phase change, and poor mechanical properties hinder its use in BTMSs.

In order to solve the above problems, scholars have developed various methods to improve the thermal conductivity of phase-change materials. Common methods include the addition of carbon powder, metal foam, carbon fiber, etc. [15–19]. Recent studies have shown that wrapping PW in a porous structure is a simple and efficient method [20–22]. EG is widely used due to its loose, porous structure and good thermal conductivity [23]. Jiang et al. [24] found that adding graphite with a mass fraction of 16 wt% to 20 wt% in paraffin not only improves the thermal conductivity of CPCM, but also improves the thermal management performance of the

battery. Li et al. [25] added EG to PW and found that its thermal conductivity is 41 times that of PW. Wang et al. [26] prepared a copper foam/PW composite phase-change material. The addition of copper foam increases the internal heat transfer of the paraffin and reduces the energy storage time by more than 40%. Lv et al. [27] added EG to polyethylene glycol, and the results showed that the addition of EG greatly improved the thermal conductivity and heat transfer of the PCM. Jiang et al. [28] added CF to paraffin, and the results show that the thermal conductivity of the composite is almost linear with the volume fraction of carbon fiber. Compared with pristine paraffin, the in-plane thermal conductivity of the CPCM is increased by 18–57 times, and the thermal conductivity outside the surface is increased by 3.7–5.5 times.

Due to the easy leakage during the paraffin phase transition, it will affect the heat storage capacity of the PCM. Therefore, the researchers proposed some leak control methods for PCMs. Tang et al. [29] added HDPE to the MA to prevent leakage during the phase change. The results show that when the MA mass fraction is less than 70%, the MA is uniformly absorbed by the HDPE during the melting process without leakage. Lv et al. [30] used PW in the pores of nanosilica to prevent the migration and leakage of paraffin during the phase change. The addition of silica greatly improves the uniformity of the paraffin and alleviates the leakage and volume change of the paraffin. Li et al. [31] encapsulated PW/EG CPCM with silica gel, effectively preventing leakage of PW during solid-liquid phase transition. Xu and Li [32] prepared PW/diatomite/WMCNTs for a heat storage cement-based CPCM. The addition of WMCNTs not only improves the thermal conductivity of the material but also increases the heat storage and heat release rate of the material.

In addition to the above thermal conductivity and leakage problems, the mechanical properties and heat transfer properties of PCMs are also the focus of attention. After the phase-change material undergoes repeated solid-liquid circulation, shape changes or cracks may occur, which may reduce the performance and heat dissipation of the PCM. When the latent heat stored in the PCM or CPCM cannot be dissipated from the battery in time, the service life and performance of the battery may drop sharply after rapid charging or multiple cycles [33]. In this study, a new type of shape-stable composite phase-change material is proposed. PW was used as the phase-change material, EG and HDPE were used as support materials, CF as a thermal conductive additive, and 3D Al-Hc is added. The PW is dispersed into EG and CF to increase the thermal conductivity of the PCM; among them, EG is both a matrix and a strong thermal conductivity. HDPE is added to the PCM to prevent the leakage of the molten PW. Finally, PCMs made from the above various materials have good mechanical properties and heat dispersibility.

2. Materials and Experiment

2.1. Materials. The PW was provided by *Hangzhou Luer Energy Technology Co., Ltd., China*. The EG was purchased from *Shandong Qingdao Graphite Co., Ltd.*, China. The CF was purchased from *Fujian United New Materials Technology Co., Ltd*. The CF has a thermal conductivity of 900 W/(m·K), an average length of 15 μm, and a density of 2.22 g/cm^3. HDPE was supplied by *Qatar Petrochemical Company* with a density of 0.953 g/cm^3 and a softening point of 126°C. The AL-Hc panel was provided by *Shanghai Luhuan Industrial Co., Ltd*. The 3D AL-Hc and the AL-Hc panels are regular hexagons having a side length of 3 mm and a height of 5 mm, and both have a thickness of 0.4 mm, respectively. The 3D AL-Hc is evenly distributed with five cylinders, each having a height of 10 mm, a diameter of 3 mm, and an angle of 45° to the wall. *Changsha New Materials Industry Research Co., Ltd*. assisted in the printing of the 3D AL-Hc. The rectangular ternary lithium battery (50 Ah) was provided by *Jiangxi Xingying Technology Co., Ltd*.

2.2. Sample Preparation. Figure 1 is the optical image of the 3D printed aluminum honeycomb with a prickly structure and aluminum honeycomb, and both are made of pure aluminum. Figure 2 is a schematic diagram of the various manufacturing techniques for preparing PW/EG/CF/HDPE CPCM and PW/EG/CF/HDPE/3D Al-Hc CPCM samples by melt blending. Figure 2(a) is a schematic diagram of the preparation process of the PW/EG/CF/HDPE powder. Figure 2(b) shows the process of preparing a CPCM plate by placing PW/EG/CF/HDPE powder and Al-HC in a mold under a tablet press pressure; in the prepared sample, each hexagonal hole of the aluminum honeycomb was filled with PW/EG/CF/HDPE CPCM. The expandable graphite powder was placed in a vacuum oven at 60°C for 24 hours. Then, it was placed in a horse boiling furnace at 800°C and rapidly expanded for 60 s to obtain the EG. HDPE and paraffin in different proportions are stirred in the molten state and thoroughly mixed. A small amount of antioxidant 1010 was added to prevent the thermal oxidative degradation of the paraffin and HDPE. Then, EG and CF were added to the mixture and stirring was continued for 60 minutes. Finally, the mixture was placed in a square mold and a pressure of 6 MPa was applied, followed by compression molding, cooling at room temperature, and then demolding. Table 1 lists the composition of the six samples.

2.3. Performance Characterization and Testing of Samples

2.3.1. Sample Characterization. Scanning electron microscopy (SEM, Hitachi s-3400 n) was utilized to observe the morphology and microstructure of the composites. The crystal structure of each CPCM was analyzed using X-ray diffraction (Bruker D8 Focus, Germany) at a scanning speed of 10°/min, CuKα = 0.154 nm, and a 2-Theta value of 10° to 80°. A 25 mm × 25 mm × 5 mm rectangular parallelepiped specimen was measured using an electronic universal testing machine under the control of a microcomputer (WDW-100E, Jinan, China) for the mechanical durability compressive strength test. The accuracy of the measurements is ±0.5%.

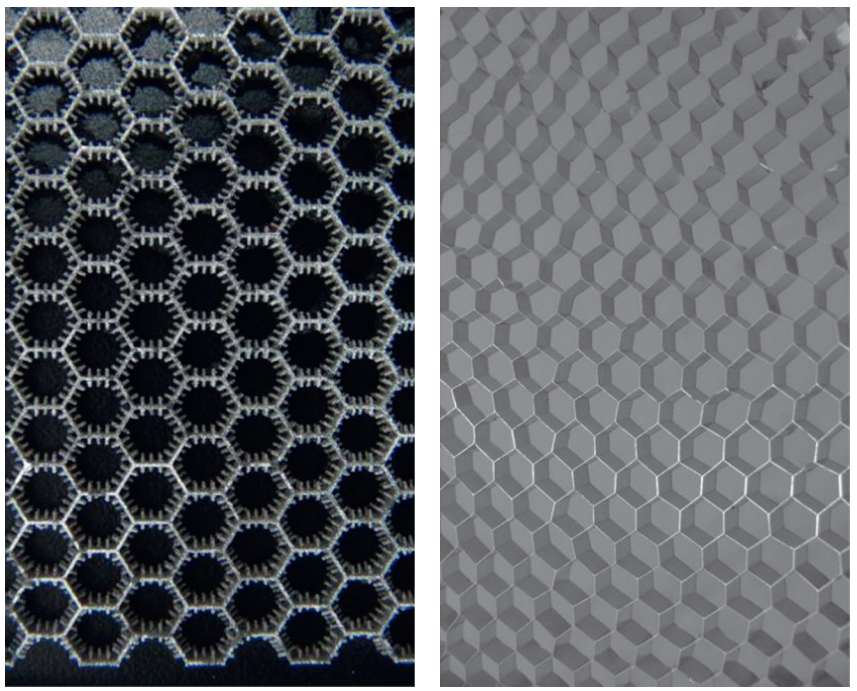

(a) (b)

Figure 1: Honeycomb. (a) 3D printing with prickly aluminum honeycomb. (b) Aluminum honeycomb.

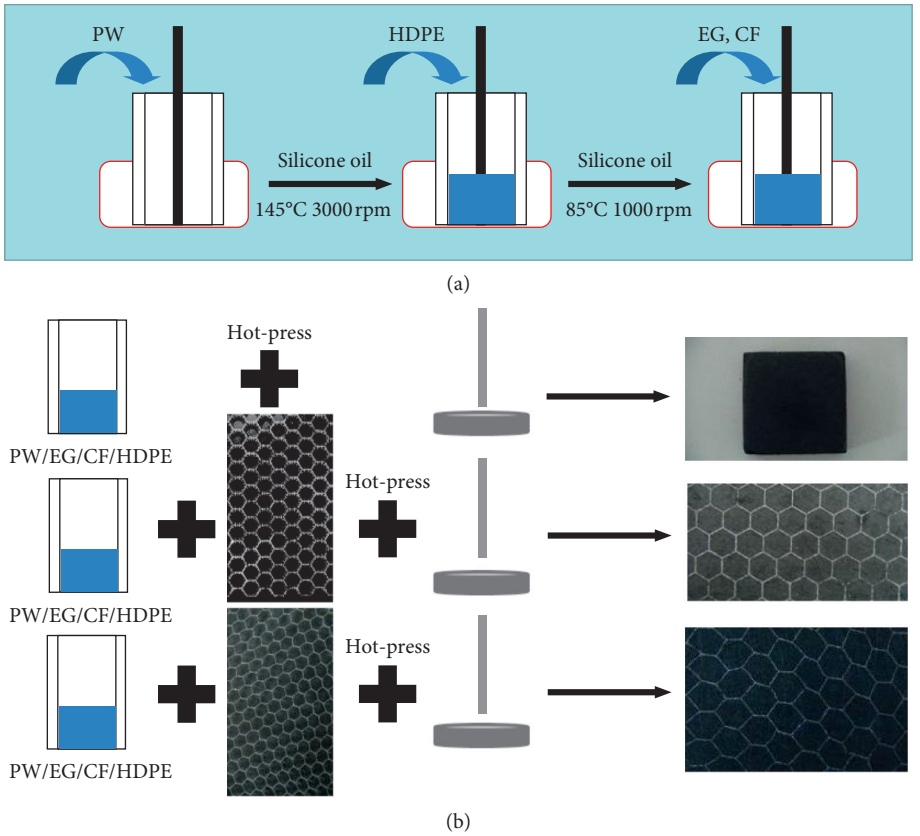

Figure 2: Schematic of the PW/EG/CF/HDPE and PW/EG/CF/HDPE/3D Al-Hc composite samples that were formed by melt mixing. (a) Schematic diagram of the preparation process of the PW/EG/CF/HDPE. (b) Preparation of the CPCM samples.

Table 1: The compositions of the PW/EG/CF/HDPE composites.

Sample	PW (wt%)	EG (wt%)	HDPE (wt%)	CF (wt%)
CPCM-CF0	93	7	0	0
CPCM-CF0.5	86.5	7	6	0.5
CPCM-CF1.5	85.5	7	6	1.5
CPCM-CF3	84	7	6	3
CPCM-CF4.5	82.5	7	6	4.5
CPCM-CF6	81	7	6	6

2.3.2. Thermal Performance Test of the Sample. The PW/EG and PW/EG/CF/HDPE composite phase-change materials were tested using a differential scanning calorimeter (DSC8000, PE Instrument Inc., USA), and the samples were heated and cooled at a rate of 5°C/min under an N_2 atmosphere. The temperature test range was 10–70°C. The thermal conductivity of the sample was measured with a TC 3000 type thermal conductivity meter at a room temperature of 25°C. The sensor was placed between two identical samples and pressed with a weight. This method has the advantages of fast detection speed, high accuracy, and simple sample preparation. Thermogravimetric analysis (TGA, Model 4000, USA) was used at a heating rate of 10°C/min in N_2 atmosphere at room temperature to 700°C with a sensitivity of 0.1 mg.

2.4. Construction of Ternary Lithium Battery Thermal Response Platform. Figure 3 shows the experimental platform for applying the CPCM to the thermal response of a ternary lithium battery cooling module. The charge and discharge cycle of the battery at different discharge rates were achieved by using a constant-wing battery charging and discharging system (5V200A-1CH, Shenzhen, China). This was performed by attaching the CPCM to the surface of the ternary lithium battery, which was subject to different discharge rates, using a HIOKI data storage recorder (MR8875-30A, Shanghai, China) in a high-low temperature test chamber at a constant temperature of 25°C. Table 2 shows the key data during battery charging and discharging, and C represents the capacity of the battery.

3. Results and Discussion

3.1. Microscopic Appearance. The microphotographs of the CF, HDPE, PW/EG, and PW/EG/CF/HDPE CPCM samples are shown in Figure 4. As shown in Figure 4(a), the surface of the carbon fiber is very smooth, and the outer diameter is consistent with the diameter that is provided by the supplier. Figure 4(b) is a microscopic topography of the high HDPE. Figure 4(c) is a microscopic topography of the PW/EG CPCM. The results in the figure indicate that PW is completely adsorbed in the pore structure of EG. Figure 4(d) is a microstructure diagram of a PW/EG/CF/HDPE CPCM. In this CPCM, PW, EG, and HDPE are mixed, and CF is uniformly dispersed in the CPCM.

3.2. Leakage Rate. Figure 5 is an optical image of the PW/CF/HDPE CPCM and PW/EG/CF/HDPE CPCM after 2 hours in the incubator. As can be seen from the figure, there is no significant leakage of paraffin in the PW/EG/CF/HDPE CPCM compared to the PW/CF/HDPE CPCM, since the PW is held in place by the surface tension and capillary force of the EG. Figure 6 shows the effect of the CF content on the leakage rate of the CPCM. With the increase in the amount of CF, the leakage rate of CPCM has been reduced. However, when the CF mass fraction was 6%, the leakage rate of the CPCM was increased. As the CF content increases, a part of the CF will be agglomerated, which can destroy the crystalline structure of the PW and increase the leakage rates. In addition, it can be seen that the PCM leakage rate increases rapidly at the beginning 20 hours. However, after 20 hours, the rate of the increase in the leakage rate slowed down. This is because the paraffin on the surface of the PCM leaks quickly when heated, resulting in a rapid increase in the PCM leakage rate. The PW inside the PCM has a slower migration rate due to the superior adsorption capacity of the HDPE and EG, which decelerates the rate of increase in leakage rate after 20 hours.

3.3. Thermal Performance Analysis. The DSC curves for the PW and CPCM are shown in Figure 7. The peaks of PW/EG and PW/EG/CF/HDPE composites were lower than those of the pristine paraffin, which is attributed to the decrease in the mass fraction of the PW that is present in the composites. In addition, with the addition of the EG and CF to the PW, the exothermal peaks shifted to higher temperatures during solidification, and the exothermal peaks shifted to lower temperatures during the melting. The results show that the addition of CF to the CPCM can reduce the degree of supercooling. The latent heat value of the sample was obtained by integrating the DSC curve, as shown in Table 3. From the data in the table, the supercooling of the CPCM-CF4.5 was reduced by 51.5% and 43.3%, respectively, compared to the supercooling of the PW PCM and PW/EG CPCM. The reduction in the supercooling shortens the phase-transition period and improves the use efficiency of the composite phase-change material.

Figure 8 shows the XRD patterns of different materials, in which HDPE, CF, and PW/EG show obvious diffraction peaks at 2-Theta = 23.3°, 26.4°, 23.3°, 19.3°, 23.3°, 24.8°, and 26.4°. The XRD curve of the PW/EG/CF/HDPE CPCM showed the same diffraction peak at the same 2-Theta value. No clear new peaks were observed, thus indicating that the interaction in the PW/EG/CF/HDPE CPCM involved simple physical loading between the PW, EG, CF, and HDPE rather than chemical interaction.

Figure 9 shows the TG curves of the PW, HDPE, PW/EG, and PW/EG/CF/HDPE composite phase change materials. Degradation of the pure component is accomplished in one step, while the degradation of the blend is accomplished in two steps: the first step is the degradation of the PW; the second step is the degradation of the HDPE. This degradation behavior is mainly due to the fact that the blends are immiscible and the components have different degradation temperatures. PW starts to decompose at approximately 180°C, and this is completed at approximately 320°C. HDPE has good thermal stability, starts to decompose at approximately 450°C, and completely decomposes at

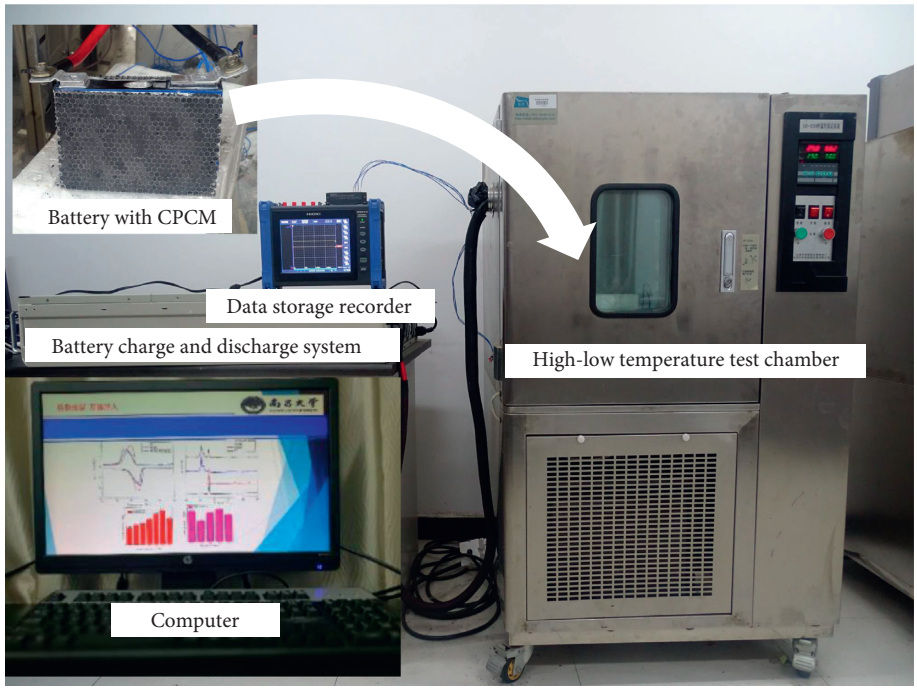

Figure 3: The experimental setup for evaluating the thermal response of the ternary lithium battery cooling module with the CPCM.

Table 2: Charge/discharge procedures.

Process	Current (A)		Voltage (V)
Charge	Calvanostatic	2	4.2 (cut-off voltage)
	Potentiostatic	0.1 (cut-off current)	—
Discharge	—	125(2.5°C)	—

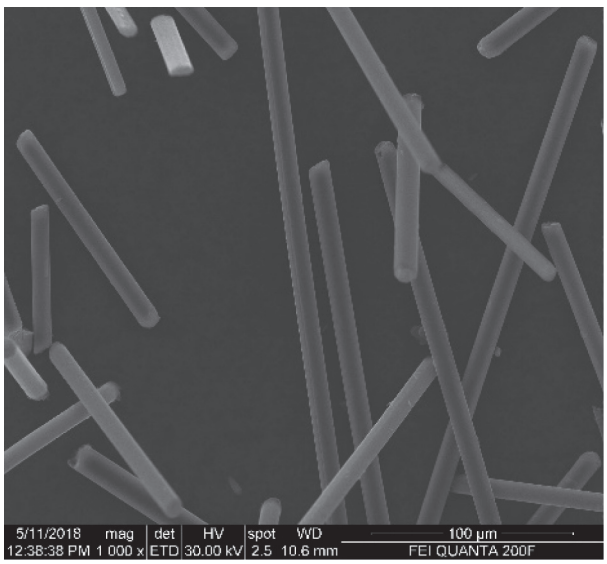

(a)

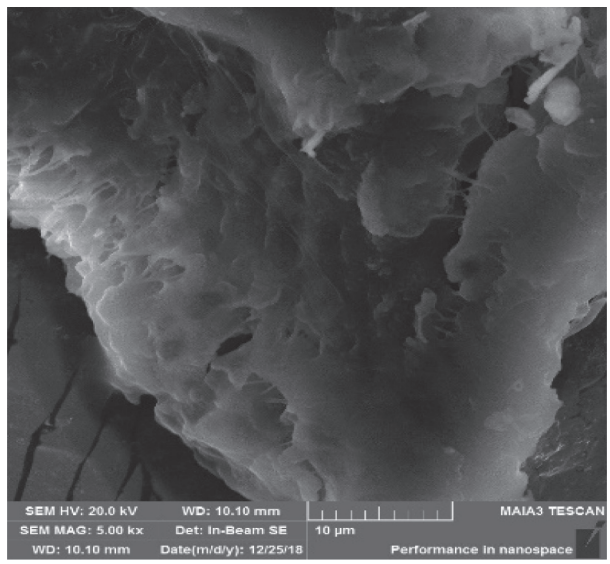

(b)

Figure 4: Continued.

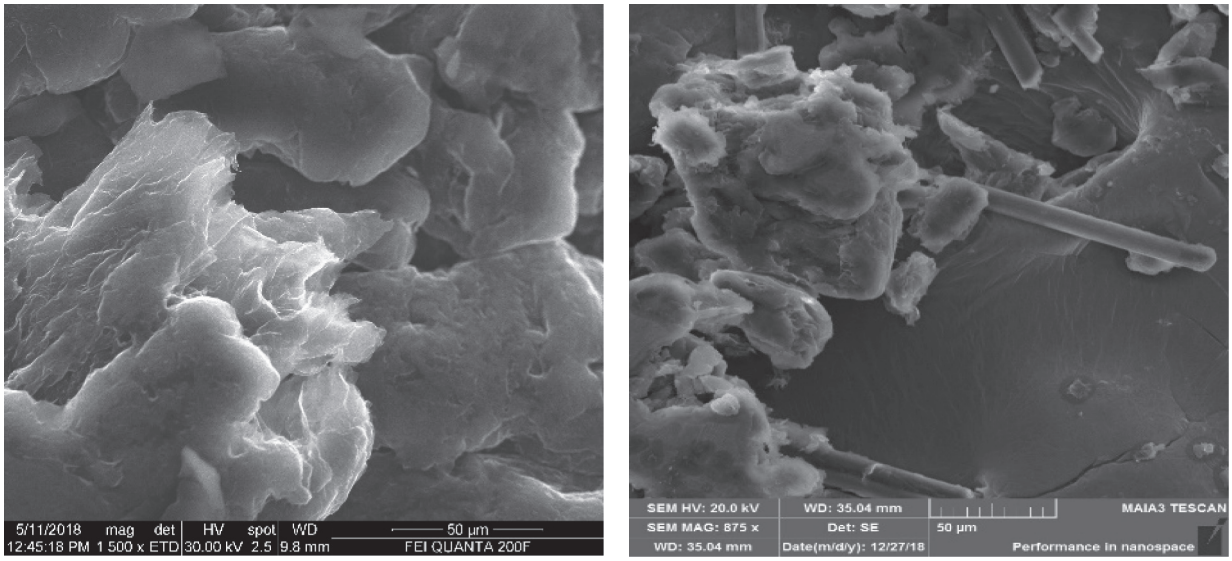

(c) (d)

Figure 4: SEM micrographs of (a) CF, (b) HDPE, (c) PW/EG, and (d) PW/EG/CF/HDPE.

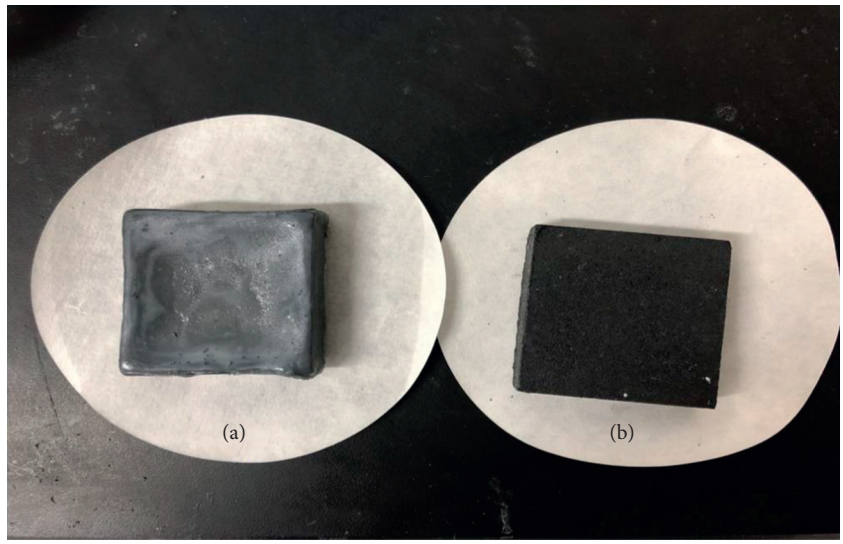

Figure 5: Sample leakage rates of the (a) PW/HDPE/CF and (b) PW/EG/CF/HDPE.

approximately 500°C. The PW/EG/CF/HDPE completes the first degradation at 190°C–330°C. This stage is the degradation of the paraffin, and the second degradation is completed at 450°C–480°C. This stage is the degradation of the HDPE. The CPCM mass residue is the same as the EG and CF contents, thus indicating that EG and CF do not degrade at approximately 500°C.

3.4. Thermal Conductivity Analysis. Thermal conductivity is an important parameter that affects the rate at which a phase-change material stores and releases heat. Figure 10 shows the thermal conductivities of the PW and CPCM with different CF mass fractions. The thermal conductivity of pristine CPCP-CF0 at room temperature was 3.03 W/(m·K). The thermal conductivity of the CPCM increases with the introduction of CF, and the thermal conductivity of CPCM-CF4.5 was 1.31 times that of CPCM-CF0. However, as the mass fraction of CF increases, the thermal conductivity drops to 3.575 W/(m·K). This is due to the presence of excessive CF agglomerates in the phase-change material. The agglomerated CF may affect the crystal structure of the PW and reduce the thermal conductivity of the phase-change material [34]. The thermal conductivity of CPCM-CF4.5-Al-Hc and CPCM-CF4.5-3D Al-Hc CPCM was measured in the same manner. The results show that the thermal conductivity increases to 4.465 W/(m·K) and 5.723 W/(m·K), which are 1.48 times and 1.9 times that of PW/EG, respectively.

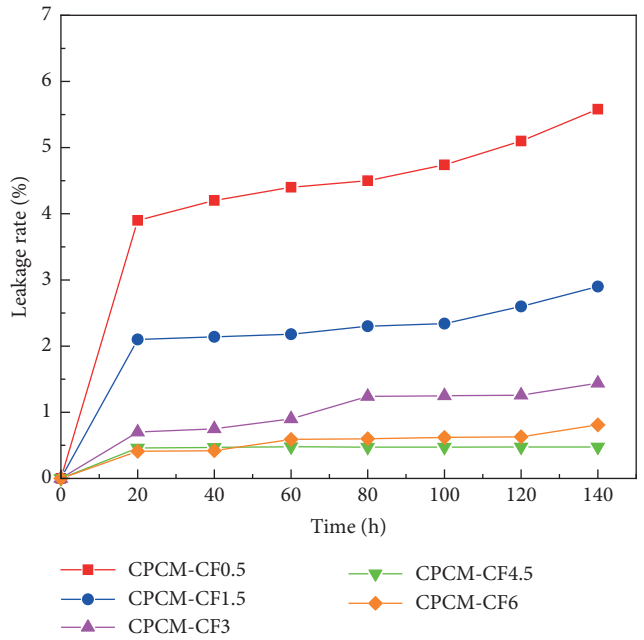

Figure 6: The leakage rates of the CPCMs.

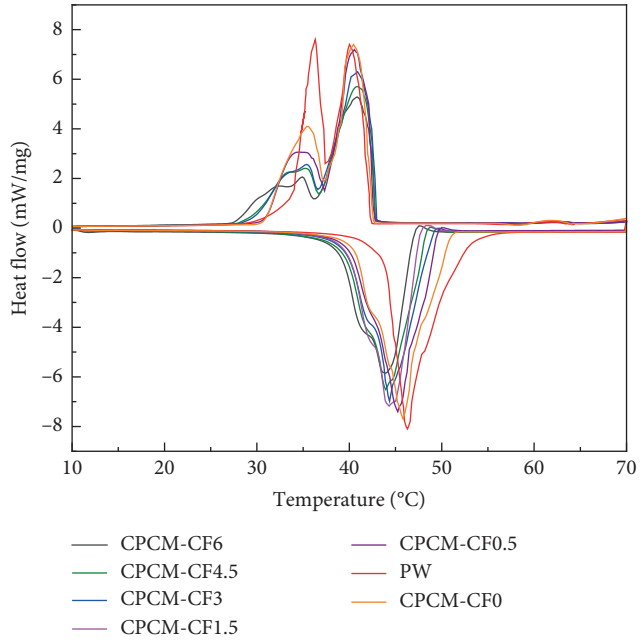

Figure 7: DSC curves of the PCM and CPCM.

Table 3: The phase-transition parameters of the samples.

Samples	Melting		Freezing	
	T_M (°C)	H_M (J/g)	T_F (°C)	H_F (J/g)
CPCM-CF0	45.8	236.3	40.5	234.2
CPCM-CF0.5	45.2	218.2	40.8	218.7
CPCM-CF1.5	44.3	222.7	41.1	217.6
CPCM-CF3	44.1	209.4	41.3	208.1
CPCM-CF4.5	43.9	208.8	41.5	202.8
CPCM-CF6	43.6	200.4	41.7	189.8

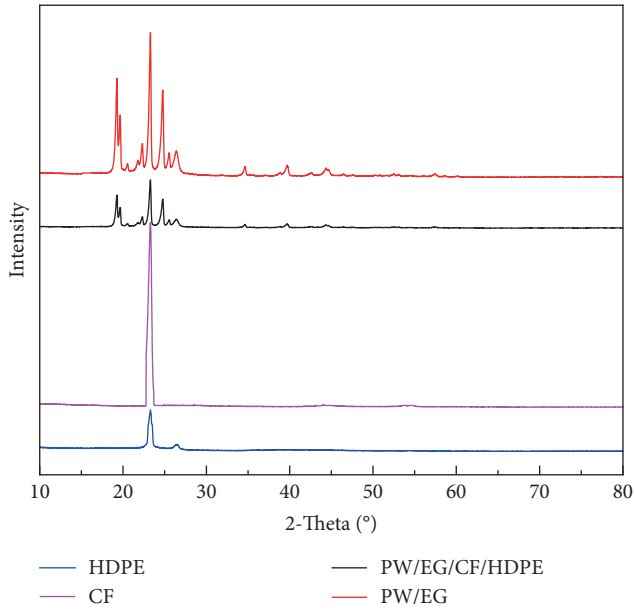

Figure 8: XRD curves of the HDPE, CF, PW/EG, and PW/EG/CF/HDPE.

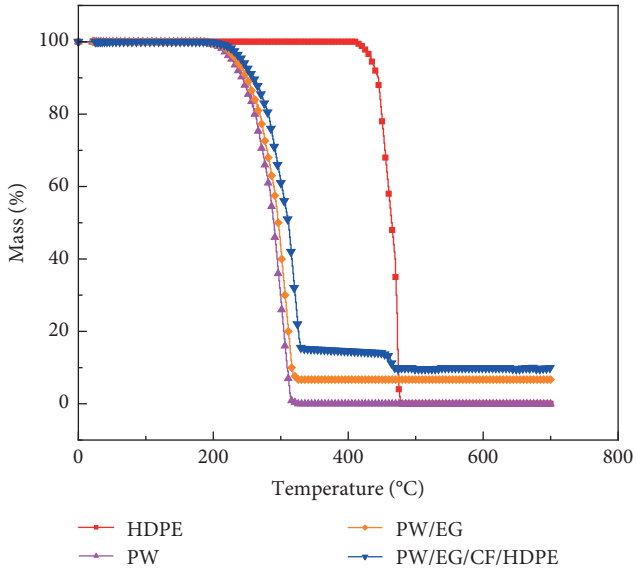

Figure 9: TG curves for the PW, HDPE, PW/EG, and PW/EG/CF/HDPE.

Therefore, it can be concluded that the thermal conduction of the CPCM-CF4.5 sample was enhanced by the addition of the aluminum honeycomb panel, and 3D Al-Hc panels have better thermal conductivity than ordinary aluminum honeycomb panels, This may be because of the following: (1) the 3D Al-Hc foil's thickness is 0.4 mm; and (2) the 3D printed aluminum honeycomb has a prickly structure, which increases the contact area with the CPCM.

3.5. Mechanical Strength Analysis. Figure 11 is a graph of the stress-strain curve of the three CPCM specimens after the compressive strength test. The strain of the three specimens increased with the increase of the applied stress, but the deformation of CPCM-CF4.5-3D Al-HC under the same stress was the smallest. Under the pressure of 100 KPa, the deformation of the PW/EG/CF/HDPE, PW/EG/CF/HDPE/Al-Hc, and PW/EG/CF/HDPE/3D Al-Hc composite panels was 8 mm, 4.9 mm, and 1.25 mm, respectively. During the test, all three samples were not crushed, indicating that the PW/EG/CF/HDPE CPCM plate has good toughness. The PW/EG/CF/HDPE/3D Al-Hc composite board had almost no deformation, which indicates that the 3D Al-Hc panel greatly improves the compressive strength of the CPCM panel.

3.6. Battery Surface Thermal Response Analysis. Figure 12 shows the temperature variation curves with a 2.5°C discharge rate for the battery surface. It can be seen from the diagram that the temperature is almost linear with time

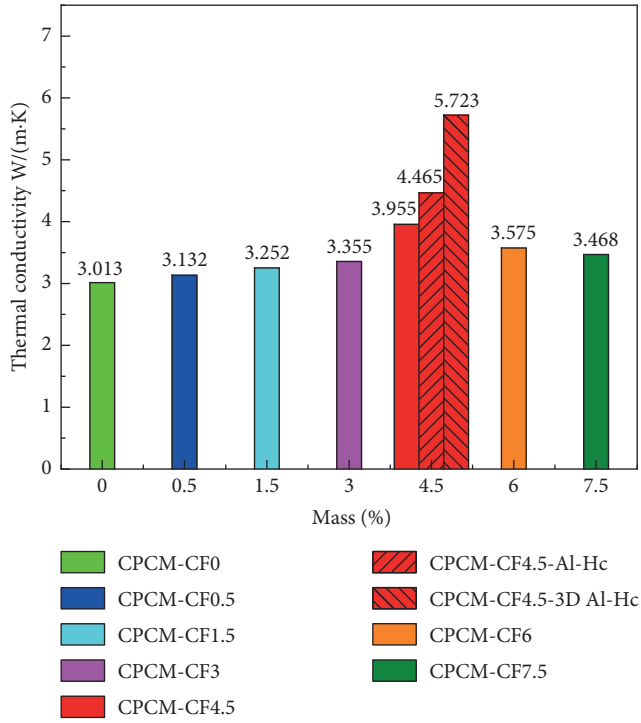

Figure 10: Thermal conductivity of the CPCM with different CF mass fractions.

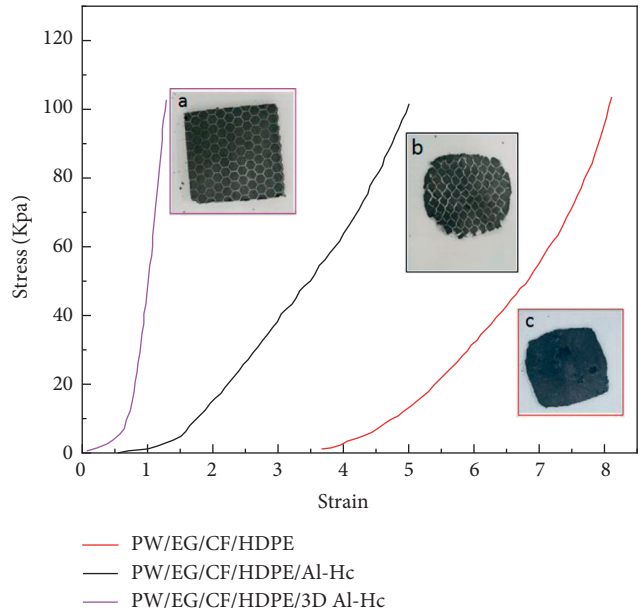

Figure 11: Stress-strain curves and images of the CPCM specimens after the compression strength test. (a), (b), and (c) are the images of the samples after the compression strength test.

when there is no PCM on the surface of the battery. At the end of the discharge, the maximum temperature reaches 71.2°C, which far exceeds the safe temperature of the battery (50°C). The temperature variations of the battery containing the CPCMs were divided into three distinct stages. At the beginning of the discharge, the surface temperature of the battery rises at a relatively fast rate. The solid CPCM is in the sensible heat cooling process, and direct thermal conduction is the dominant heat transfer mechanism. In the second stage, the temperature is maintained at approximately 42.3°C, which is within the phase-transition temperature range of the CPCM. At the end of the discharge, since the CPCM is completely dissolved, and the heat exchange rate between the CPCM and the air is slow, the surface temperature of the battery rises rapidly. However, the maximum surface temperature of the PW/EG/CF/HDPE/3D Al-Hc

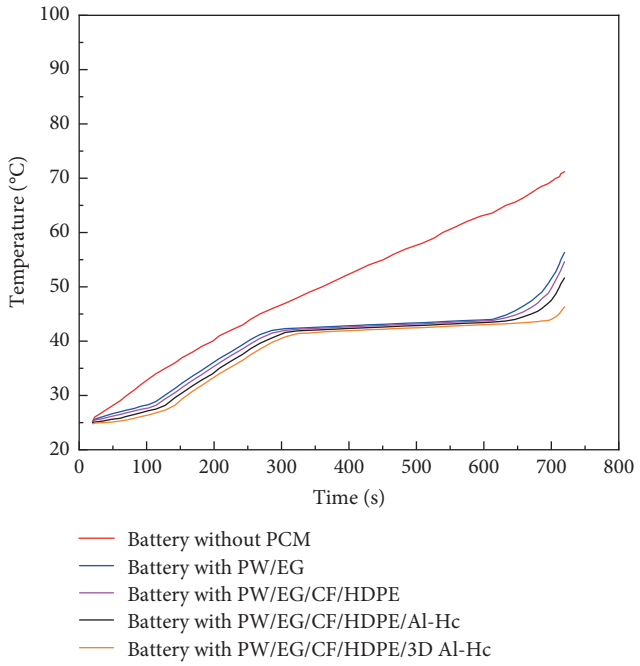

Figure 12: Temperature variations with time for the battery surface at a 2.5°C discharge rate.

CPCM battery is kept below 50°C, and it is maintained in the safe temperature range until the end of discharge. Then, the heat that is generated by the battery began transferring to the CPCM, and the CPCM began to melt. At the third stage, the surface temperature of the battery rises rapidly, and the CPCM is completely dissolved. These systems could not transfer heat from the battery into the air fast enough. However, the highest temperature of the battery incorporating the PW/EG/CF/HDPE/3D Al-Hc CPCM remained below 50°C, which was within the optimum working temperature range up until the end of the discharge.

4. Conclusions

In this study, a PW/EG/CF/HDPE CPCM was prepared, and the effect of the mass fraction of CF on the thermal properties of the CPCM was analyzed. In addition, the mechanical properties of the 3D Al-Hc and ordinary Al-Hc in CPCM and the thermal performance of the ternary lithium battery in the thermal management system were compared. From the results of our research, the following conclusions can be drawn:

(1) From the DSC curve analysis, the degree of supercooling of the prepared PW/EG/CF/HDPE CPCM was reduced by 51.5% and 43.3%, compared to the PW and PW/EG CPCM, respectively. The reduction in supercooling shortens the phase change period and also improves the efficiency of the CPCM.

(2) When the CF mass fraction is 4.5%, the thermal conductivity of the PW/EG/CF/HDPE was 3.955 W/(m·K). After the addition of the 3D Al-Hc, the thermal conductivity increased to 5.723 W/(m·K). The results show that the introduction of 3D Al-HC greatly improves the thermal conductivity of the CPCM.

(3) The strains in all three specimens increased with the applied stress. However, under the same stress, the PW/EG/CF/HDPE/3D Al-Hc CPCM was minimal compared to the other two specimens. The results show that the compressive strength of the PW/EG/CF/HDPE is markedly improved by the addition of the 3D Al-Hc.

(4) The thermal response of the cell surface was analyzed. At an exchange rate of 2.5°C, the highest surface temperature of the battery with the PW/EG/CF/HDPE/3D Al-Hc CPCM was recorded as 45.5°C, and it remained below the safe temperature of 50°C. This is attributed to the fact that the metal framework that is provided by the 3D Al-Hc improves the thermal conduction and heat dissipation capability of the CPCM.

Data Availability

The data used to support the findings of this study are included within the article and are available from the corresponding author upon reasonable request.

Conflicts of Interest

The authors declare that they have no conflicts of interest.

Acknowledgments

This study was supported by a grant from the National Science Foundation of China (no. 51762034), Scientific and Technological Project of Education Department, and Natural Science Foundation of Jiangxi Province, China (grant nos. KJJ170930 and 20181BAB206032).

References

[1] J. He, X. Yang, and G. Zhang, "A phase change material with enhanced thermal conductivity and secondary heat dissipation capability by introducing a binary thermal conductive skeleton for battery thermal management," *Applied Thermal Engineering*, vol. 148, pp. 984–991, 2019.

[2] S. Hong, X. Zhang, K. Chen, and S. Wang, "Design of flow configuration for parallel air-cooled battery thermal management system with secondary vent," *International Journal of Heat and Mass Transfer*, vol. 116, pp. 1204–1212, 2018.

[3] X. M. Xu and R. He, "Research on the heat dissipation performance of battery pack based on forced air cooling," *Journal of Power Sources*, vol. 240, pp. 33–41, 2013.

[4] E. Jiaqiang, D. Han, A. Qiu et al., "Orthogonal experimental design of liquid-cooling structure on the cooling effect of a liquid-cooled battery thermal management system," *Applied Thermal Engineering*, vol. 132, pp. 508–520, 2018.

[5] F. He, A. A. Ams, Y. Roosien, W. Tao, B. Geist, and K. Singh, "Reduced-order thermal modeling of liquid-cooled lithium-ion battery pack for EVs and HEVs," in *Proceedings of the 2017 IEEE Transportation Electrification Conference and Expo (ITEC)*, IEEE, Chicago, IL, USA, june 2017.

[6] L. Ghadbeigi, B. Day, K. Lundgren, and T. D. Sparks, "Cold temperature performance of phase change material based battery thermal management systems," *Energy Reports*, vol. 4, pp. 303–307, 2018.

[7] A. Greco, X. Jiang, and D. Cao, "An investigation of lithium-ion battery thermal management using paraffin/porous-graphite-matrix composite," *Journal of Power Sources*, vol. 278, pp. 50–68, 2015.

[8] M. M. Farid, A. M. Khudhair, S. A. K. Razack, and S. Al-Hallaj, "A review on phase change energy storage: materials and applications," *Energy Conversion and Management*, vol. 45, no. 9-10, pp. 1597–1615, 2004.

[9] M. M. Kenisarin, "Thermophysical properties of some organic phase change materials for latent heat storage. A review," *Solar Energy*, vol. 107, pp. 553–575, 2014.

[10] X. Zhang, H. Liu, Z. Huang et al., "Preparation and characterization of the properties of polyethylene glycol @ Si_3N_4 nanowires as phase-change materials," *Chemical Engineering Journal*, vol. 301, pp. 229–237, 2016.

[11] S. Kahwaji, M. B. Johnson, A. C. Kheirabadi, D. Groulx, and M. A. White, "Fatty acids and related phase change materials for reliable thermal energy storage at moderate temperatures," *Solar Energy Materials and Solar Cells*, vol. 167, pp. 109–120, 2017.

[12] H. U. Rammelberg, T. Osterland, B. Priehs, O. Opel, and W. K. L. Ruck, "Thermochemical heat storage materials—performance of mixed salt hydrates," *Solar Energy*, vol. 136, pp. 571–589, 2016.

[13] V. G. Orlov and G. S. Sergeev, "On the nature of chemical bonding in phase change materials on the base of $(GeTe)_m$-$(Sb_2Te_3)_n$ alloys," *Solid State Communications*, vol. 258, pp. 7–10, 2017.

[14] M. Kenisarin and K. Mahkamov, "Salt hydrates as latent heat storage materials: thermophysical properties and costs," *Solar Energy Materials and Solar Cells*, vol. 145, pp. 255–286, 2016.

[15] X. Xiao, P. Zhang, and M. Li, "Preparation and thermal characterization of paraffin/metal foam composite phase change material," *Applied Energy*, vol. 112, pp. 1357–1366, 2013.

[16] Z. Ling, J. Chen, X. Fang et al., "Experimental and numerical investigation of the application of phase change materials in a simulative power batteries thermal management system," *Applied Energy*, vol. 121, pp. 104–113, 2014.

[17] F. Samimi, A. Babapoor, M. Azizi, and G. Karimi, "Thermal management analysis of a Li-ion battery cell using phase change material loaded with carbon fibers," *Energy*, vol. 96, pp. 355–371, 2016.

[18] R. Kizilel, A. Lateef, R. Sabbah, M. M. Farid, J. R. Selman, and S. Al-Hallaj, "Passive control of temperature excursion and uniformity in high-energy Li-ion battery packs at high current and ambient temperature," *Journal of Power Sources*, vol. 183, no. 1, pp. 370–375, 2008.

[19] A. Alrashdan, A. T. Mayyas, and S. Al-Hallaj, "Thermo-mechanical behaviors of the expanded graphite-phase change material matrix used for thermal management of Li-ion battery packs," *Journal of Materials Processing Technology*, vol. 210, no. 1, pp. 174–179, 2010.

[20] M. Mehrali, S. T. Latibari, M. Mehrali, H. S. C. Metselaar, and M. Silakhori, "Shape-stabilized phase change materials with high thermal conductivity based on paraffin/graphene oxide composite," *Energy Conversion and Management*, vol. 67, pp. 275–282, 2013.

[21] S. Karaman, A. Karaipekli, A. Sarı, and A. Biçer, "Polyethylene glycol (PEG)/diatomite composite as a novel form-stable phase change material for thermal energy storage," *Solar Energy Materials and Solar Cells*, vol. 95, no. 7, pp. 1647–1653, 2011.

[22] D. Sun and L. Wang, "Utilization of paraffin/expanded perlite materials to improve mechanical and thermal properties of cement mortar," *Construction and Building Materials*, vol. 101, pp. 791–796, 2015.

[23] X. Guo, S. Zhang, and J. Cao, "An energy-efficient composite by using expanded graphite stabilized paraffin as phase change material," *Composites Part A: Applied Science and Manufacturing*, vol. 107, pp. 83–93, 2018.

[24] G. Jiang, J. Huang, Y. Fu, M. Cao, and M. Liu, "Thermal optimization of composite phase change material/expanded graphite for Li-ion battery thermal management," *Applied Thermal Engineering*, vol. 108, pp. 1119–1125, 2016.

[25] Z. Li, W. G. Sun, G. Wang, and Z. G. Wu, "Experimental and numerical study on the effective thermal conductivity of paraffin/expanded graphite composite," *Solar Energy Materials and Solar Cells*, vol. 128, pp. 447–455, 2014.

[26] C. Wang, T. Lin, N. Li, and H. Zheng, "Heat transfer enhancement of phase change composite material: copper foam/paraffin," *Renewable Energy*, vol. 96, pp. 960–965, 2016.

[27] Y. Lv, W. Zhou, and W. Jin, "Experimental and numerical study on thermal energy storage of polyethylene glycol/expanded graphite composite phase change material," *Energy and Buildings*, vol. 111, pp. 242–252, 2016.

[28] Z. Jiang, T. Ouyang, Y. Yang et al., "Thermal conductivity enhancement of phase change materials with form-stable carbon bonded carbon fiber network," *Materials & Design*, vol. 143, pp. 177–184, 2018.

[29] Y. Tang, D. Su, X. Huang, G. Alva, L. Liu, and G. Fang, "Synthesis and thermal properties of the MA/HDPE composites with nano-additives as form-stable PCM with improved thermal conductivity," *Applied Energy*, vol. 180, pp. 116–129, 2016.

[30] Y. Lv, W. Situ, X. Yang, G. Zhang, and Z. Wang, "A novel nanosilica-enhanced phase change material with anti-leakage and anti-volume-changes properties for battery thermal management," *Energy Conversion and Management*, vol. 163, pp. 250–259, 2018.

[31] J. Li, J. Huang, and M. Cao, "Properties enhancement of phase-change materials via silica and Al honeycomb panels for the thermal management of $LiFeO_4$ batteries," *Applied Thermal Engineering*, vol. 131, pp. 660–668, 2018.

[32] B. Xu and Z. Li, "Paraffin/diatomite/multi-wall carbon nanotubes composite phase change material tailor-made for thermal energy storage cement-based composites," *Energy*, vol. 72, pp. 371–380, 2014.

[33] G. Jiang, J. Huang, M. Liu, and M. Cao, "Experiment and simulation of thermal management for a tube-shell Li-ion battery pack with composite phase change material," *Applied Thermal Engineering*, vol. 120, pp. 1–9, 2017.

[34] B. Tian, W. Yang, L. Luo et al., "Synergistic enhancement of thermal conductivity for expanded graphite and carbon fiber in paraffin/EVA form-stable phase change materials," *Solar Energy*, vol. 127, pp. 48–55, 2016.